Angewandte Chemie
Eine Zeitschrift der Gesellschaft Deutscher Chemiker

Supporting Information

Enhanced Drug Delivery by Dissolution of Amorphous Drug Encapsulated in a Water Unstable Metal–Organic Framework (MOF)

*Kuthuru Suresh and Adam J. Matzger**

anie_201907652_sm_miscellaneous_information.pdf

Supporting Information

SI 1. Experimental Section

Terephthalic acid (98.0%), curcumin (CUR, >98.0% curcuminoid content) and sulindac (SUL, 98.0%) were purchased from Sigma Aldrich. Triamterene (TAT, 98%) was purchased from Alfa Aesar. N,N-dimethylformamide (DMF, ACS grade), methylene chloride (DCM, HPLC grade, 99.9%), acetonitrile (ACN, HPLC grade, 99.9%) and zinc nitrate hexahydrate ($Zn(NO_3)_2 \cdot 6H_2O$, ACS grade) were purchased from Fisher Scientific. N,N-diethylformamide (DEF, 99.0%) was purchased from Acros Organics.

MOF Synthesis
MOF-5 was synthesized and activated according to the literature procedure.[1]

drug@MOF-5 composites synthesis

CUR@MOF-5 composite:
Activated MOF-5 crystals (~20 mg) were soaked in 0.3 mL of a CUR suspension (~5 mg) in DCM solution and the mixture was kept on an IKA® vibrax VXR basic shaker at room temperature for 10 days. The resultant CUR@MOF-5 composite crystals were removed by filtration and washed with DCM to eliminate residual drug from the surface of the CUR@MOF-5 composite crystals. The CUR@MOF-5composite crystals were activated by exposure to dynamic vacuum (10^{-2} Torr) at room temperature and were stored in a glove box under an atmosphere of nitrogen. The CUR@MOF-5 composite was characterized by PXRD (Figure 3b), infrared (Figure S2a) and Raman (Figure S3a) techniques.

SUL@MOF-5 composite:
Activated MOF-5 crystals (~20 mg) were soaked in 0.3 mL of a SUL suspension (~10 mg) in ACN solution and the mixture was kept on an IKA® vibrax VXR basic shaker at room temperature for 10 days. The resultant SUL@MOF-5 composite crystals were removed by filtration and washed with ACN to eliminate residual drug from the surface of the SUL@MOF-5 composite crystals. The SUL@MOF-5 composite crystals were activated by exposure to dynamic vacuum (10^{-2} Torr) at 80 °C for 2 hours and were stored in a glove box under an atmosphere of nitrogen. The SUL@MOF-5 composite was characterized by PXRD (Figure 3c), infrared (Figure S2b) and Raman (Figure S3b) techniques.

TAT@MOF-5 composite:
Activated MOF-5 crystals (~20 mg) were soaked in 0.3 mL of a TAT suspension (~10 mg) in ACN solution and the mixture was kept on a Glas-Col® shaker at 80 °C for 6 days. The resultant TAT@MOF-5 composite crystals were removed by filtration and washed with ACN to eliminate residual drug from the surface of the TAT@MOF-5 composite crystals. The TAT@MOF-5 composite crystals were activated by exposure to dynamic vacuum (10^{-2} Torr) at 80 °C for 6 hours and were stored in a glove box under an atmosphere of nitrogen. The TAT@MOF-5 composite was characterized by PXRD (Figure 3d), infrared (Figure S2c) and Raman (Figure S3c) techniques.

SI 2. Instrumental details

Powder X-ray diffraction

Powder X-ray diffraction (PXRD) data of MOF-5, CUR, SUL, TAT, and drug@MOF-5 composites as well as decomposed products in simulated gastric and PBS media were collected on a PANalytical Empyrean diffractometer in Bragg-Brentano geometry using Cu-Kα radiation (λ = 1.54187 Å), operating at 45 kV and 40 mA. The incident beam was equipped with a Bragg-BrentanoHD X-ray optic using fixed slits/soller slits. The detector was a silicon-based linear position sensitive X'Celerator Scientific operating in 1-D scanning mode. Data were collected from 5 to 50° 2θ using a step size of 0.008° and a count time of at least 10 s per step. Powder patterns were processed using Jade Plus software (Materials Data, Inc)[2] and OriginPro 8 software.

^{1}H-NMR measurement

All ^{1}H-NMR measurements were carried out on a Varian MR400 (400 MHz (9.4 Tesla) spectrometer. All the solid forms were dissolved in acidic DMSO-d_6 (500 µL DMSO-d_6 + 50 µL of 35 wt % DCl in D_2O.)

Attenuated total reflectance-infrared (ATR-IR) spectroscopy

Mid-infrared spectra for CUR, SUL, TAT, MOF-5, and drug@MOF-5 composites were collected using a Thermo Scientific Nicolet iS50 FT-IR spectrophotometer with integrated diamond attenuated total reflectance (ATR) module equipped with KBr beamsplitter and DTGS detector. Spectra were analyzed using OMNIC software. Advanced ATR correction using default parameters in the OMNIC software was used to correct the ATR spectra for the shifting of infrared absorption peaks and the effects of variation in depth of penetration.

Raman spectroscopy

The Raman spectra for CUR, SUL, TAT, MOF-5, and drug@MOF-5 composites were collected on a Renishaw inVia Raman microscope equipped with a Rencam CCD detector, 785 nm laser, 1200 lines/mm grating, and a 65 µm slit. Calibration was performed with a silicon standard in static mode. Spectra were analyzed using the WiRE 3.4 software package.

Gas sorption measurements

Sorption experiments were carried out using a NOVA *e* series 4200 surface area analyzer (Quantachrome Instruments, Boynton Beach, Florida, USA). N_2 (99.999%) was purchased from Cryogenic Gases and used as received. For N_2 measurements, a glass sample cell was charged with ~30 mg sample and analyzed at 77 K. Sorption isotherms were collected in the NOVAwin software.

SI 3. Proton NMR spectra of CUR, SUL, TAT and digested MOF-5 and drug@MOF-5 composites (Figure S1a-e)

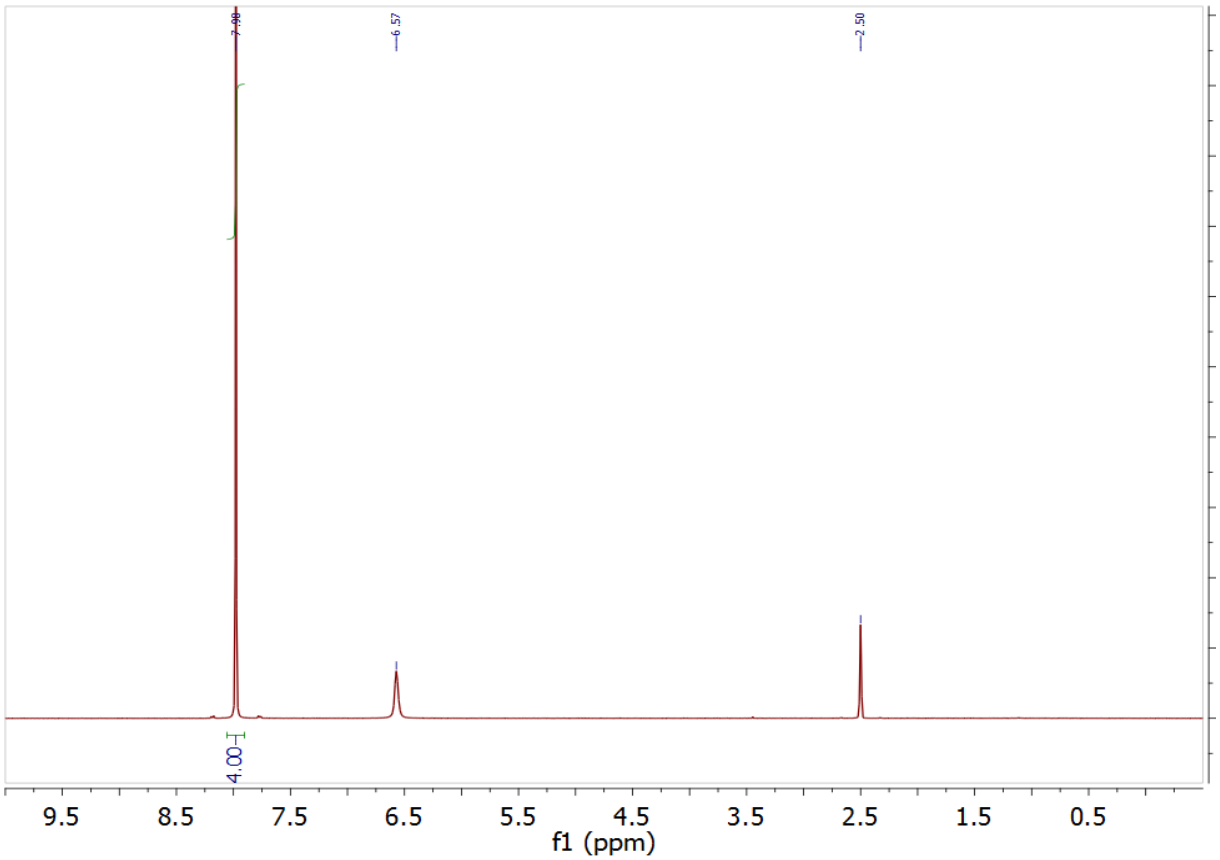

Figure S1a: Proton NMR spectrum for digested MOF-5.

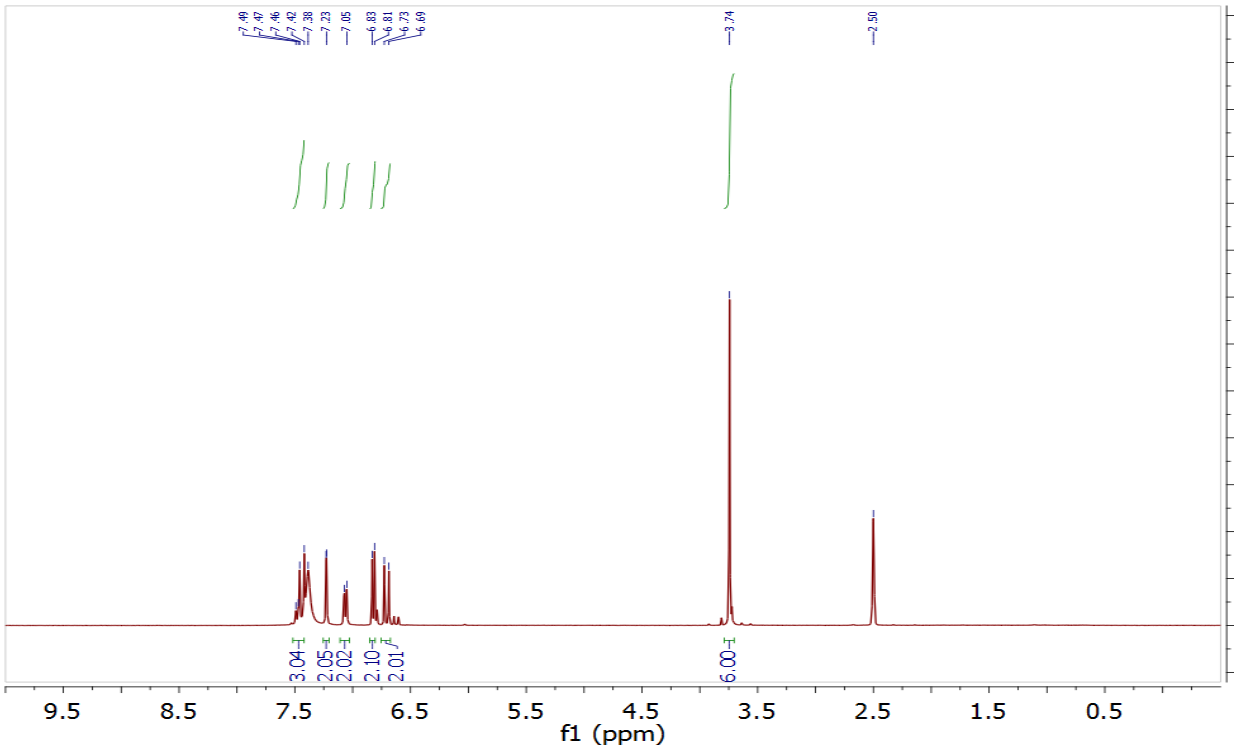

Figure S1b: CUR proton NMR spectrum.

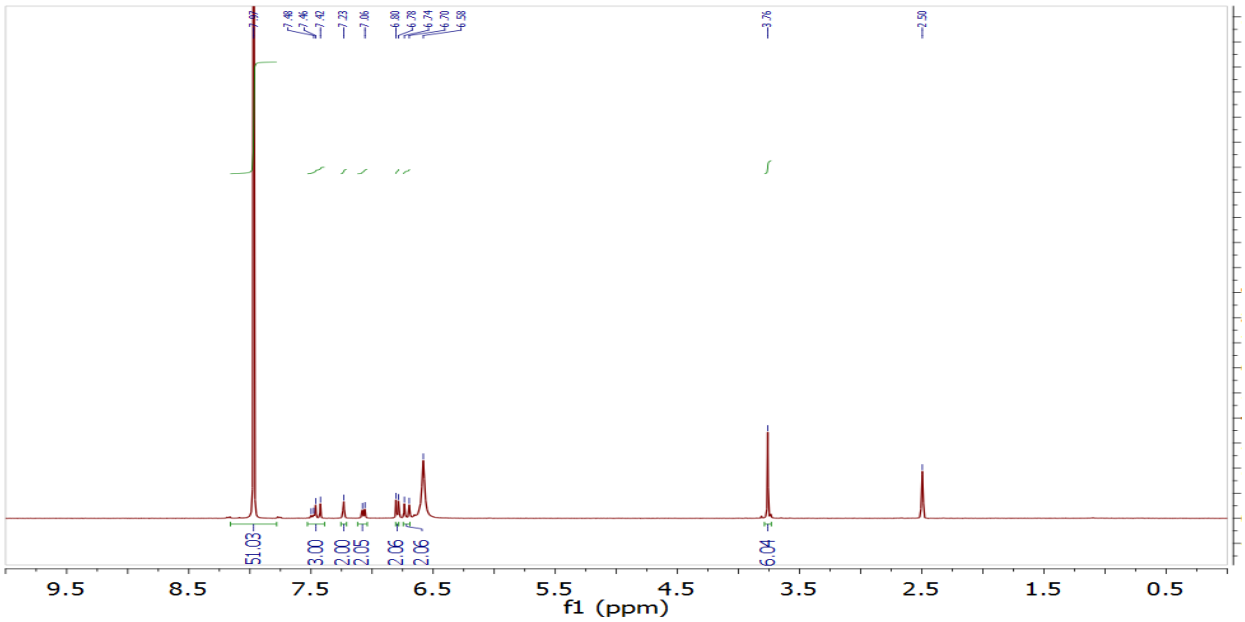

Figure S1c: Proton NMR spectrum for digested CUR@MOF-5 composite.

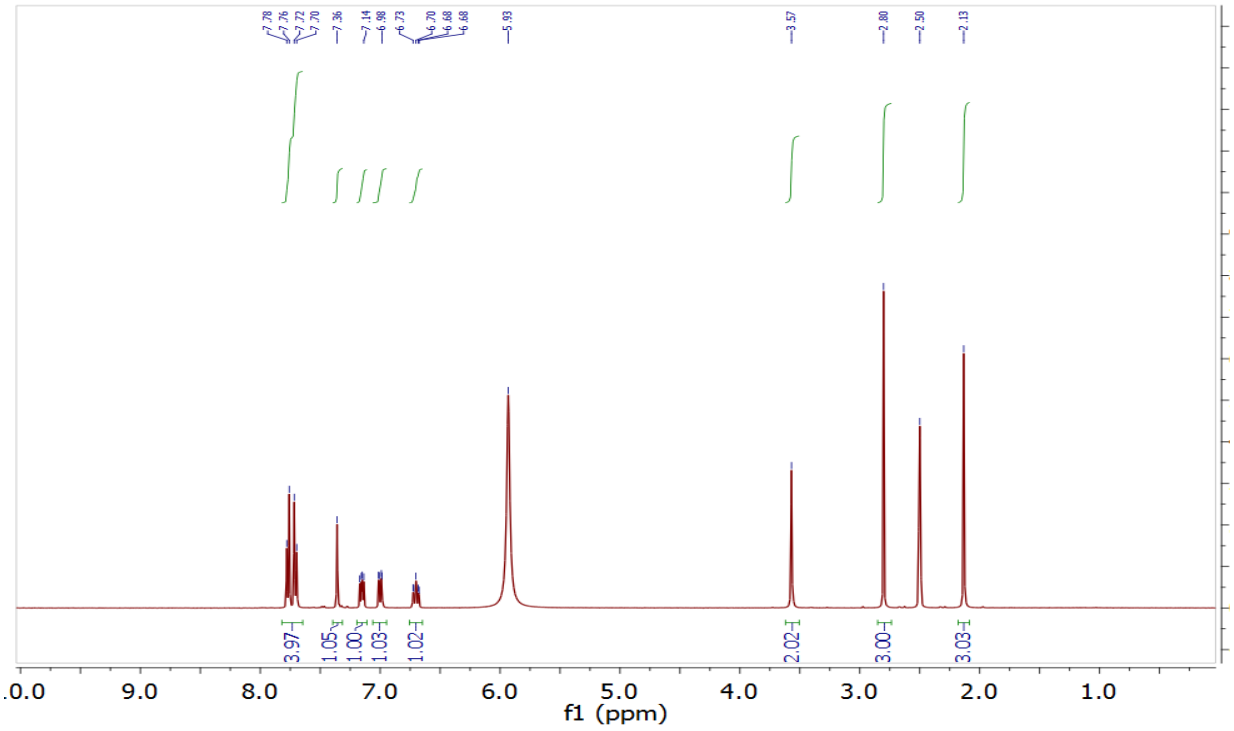

Figure S1d: SUL proton NMR spectrum.

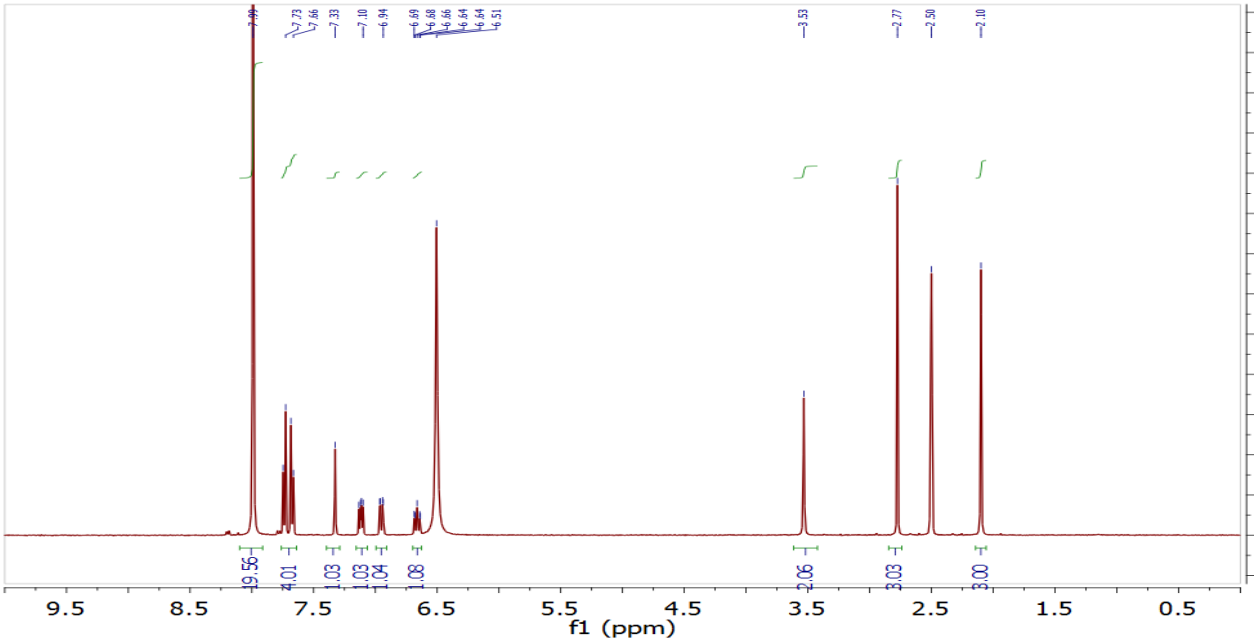

Figure S1e: Proton NMR spectrum for digested SUL@MOF-5 composite.

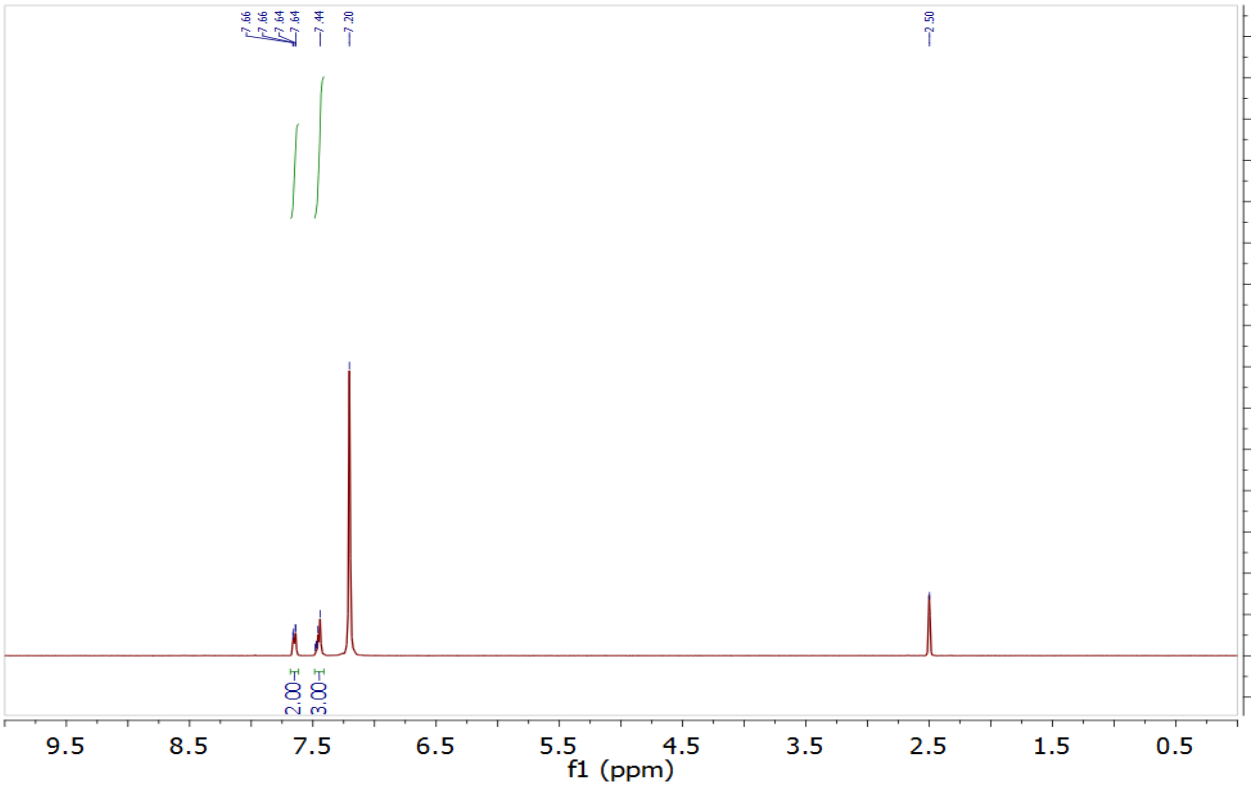

Figure S1f: TAT proton NMR spectrum.

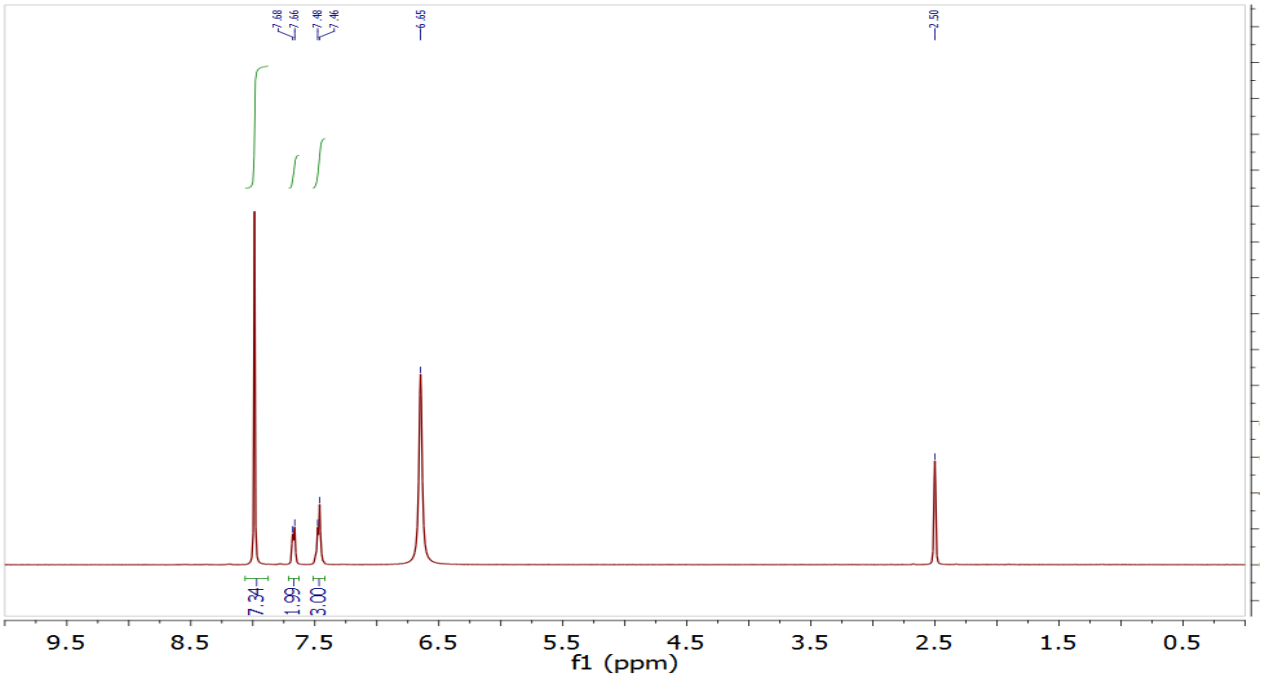

Figure S1g: Proton NMR spectrum for digested TAT@MOF-5 composite.

SI 4. IR spectra of drug@MOF-5 composites compared with their starting components (Figure S2a-b)

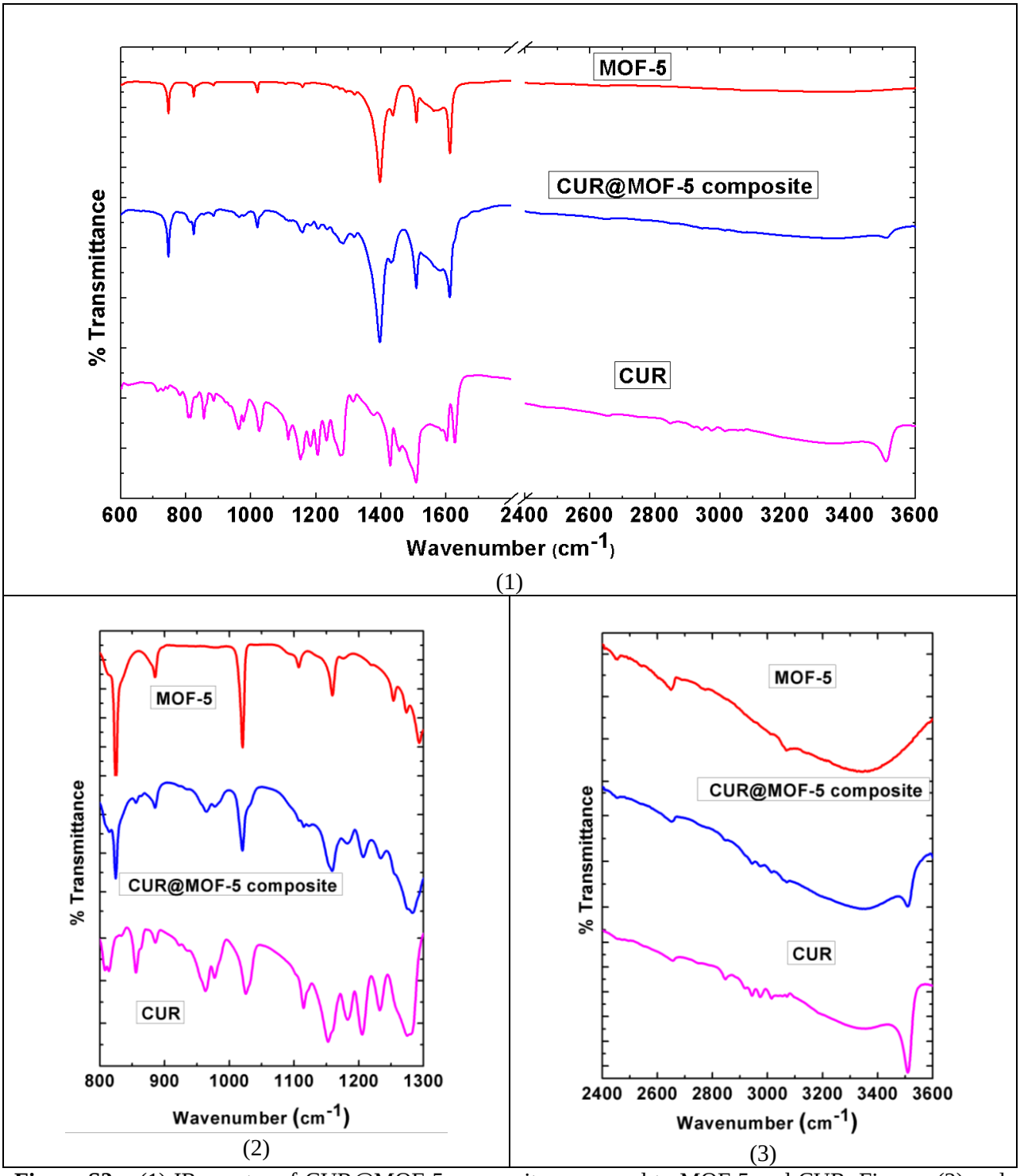

Figure S2a: (1) IR spectra of CUR@MOF-5 composite compared to MOF-5 and CUR. Figures (2) and (3) show specific spectral regions of the IR. Peaks corresponding to CUR and MOF-5 in a CUR@MOF-5 composite show strong similarities when compared to the starting components, although peak shifts are evident in MOF-5 as well as for CUR.

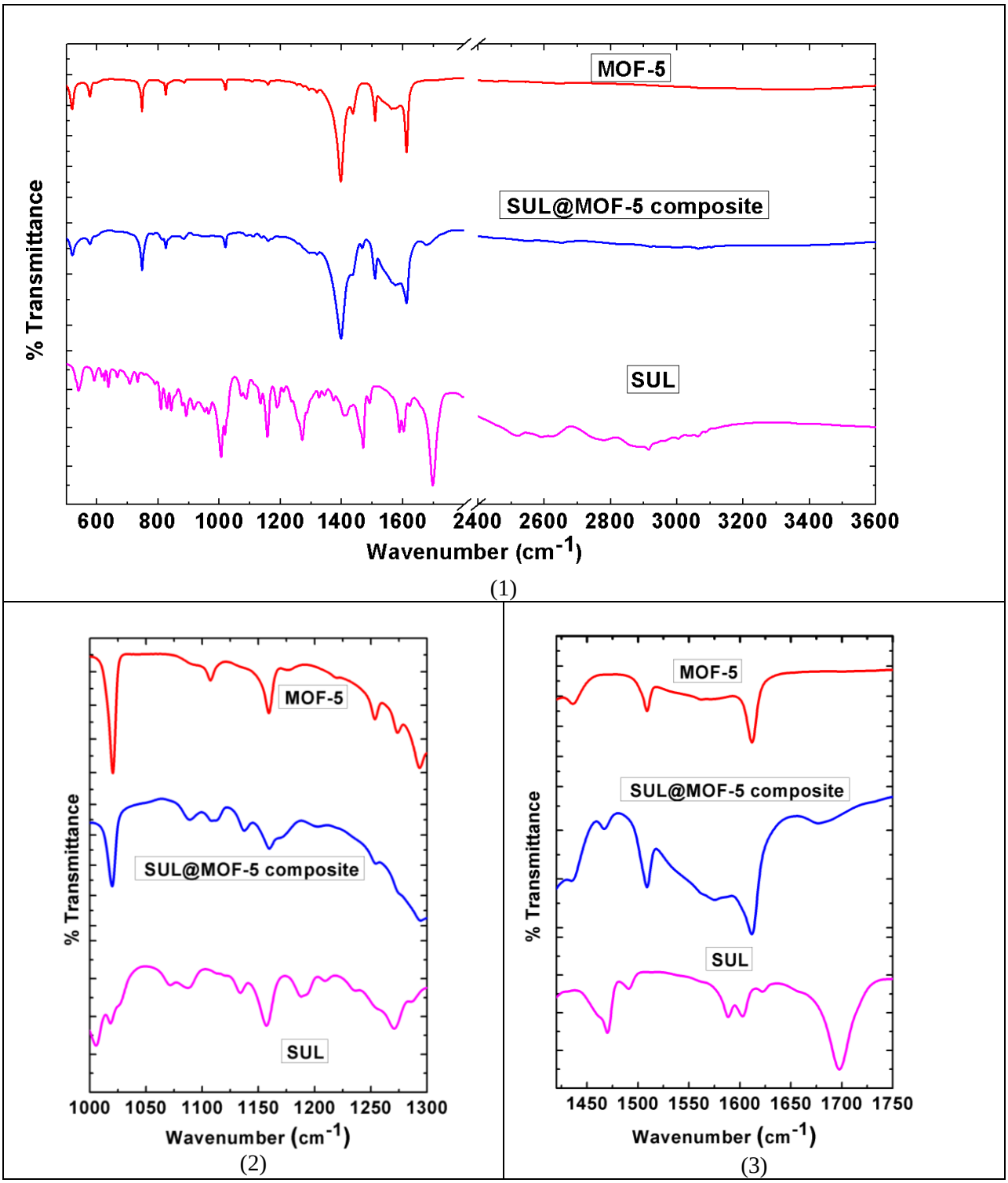

Figure S2b: (1) IR spectra of SUL@MOF-5 composite compared to MOF-5 and SUL. Figures (2) and (3) show specific spectral regions of the IR. Peaks corresponding to SUL and MOF-5 in a SUL@MOF-5 composite show strong similarities when compared to the starting components, although peak shifts are evident in MOF-5 as well as for SUL.

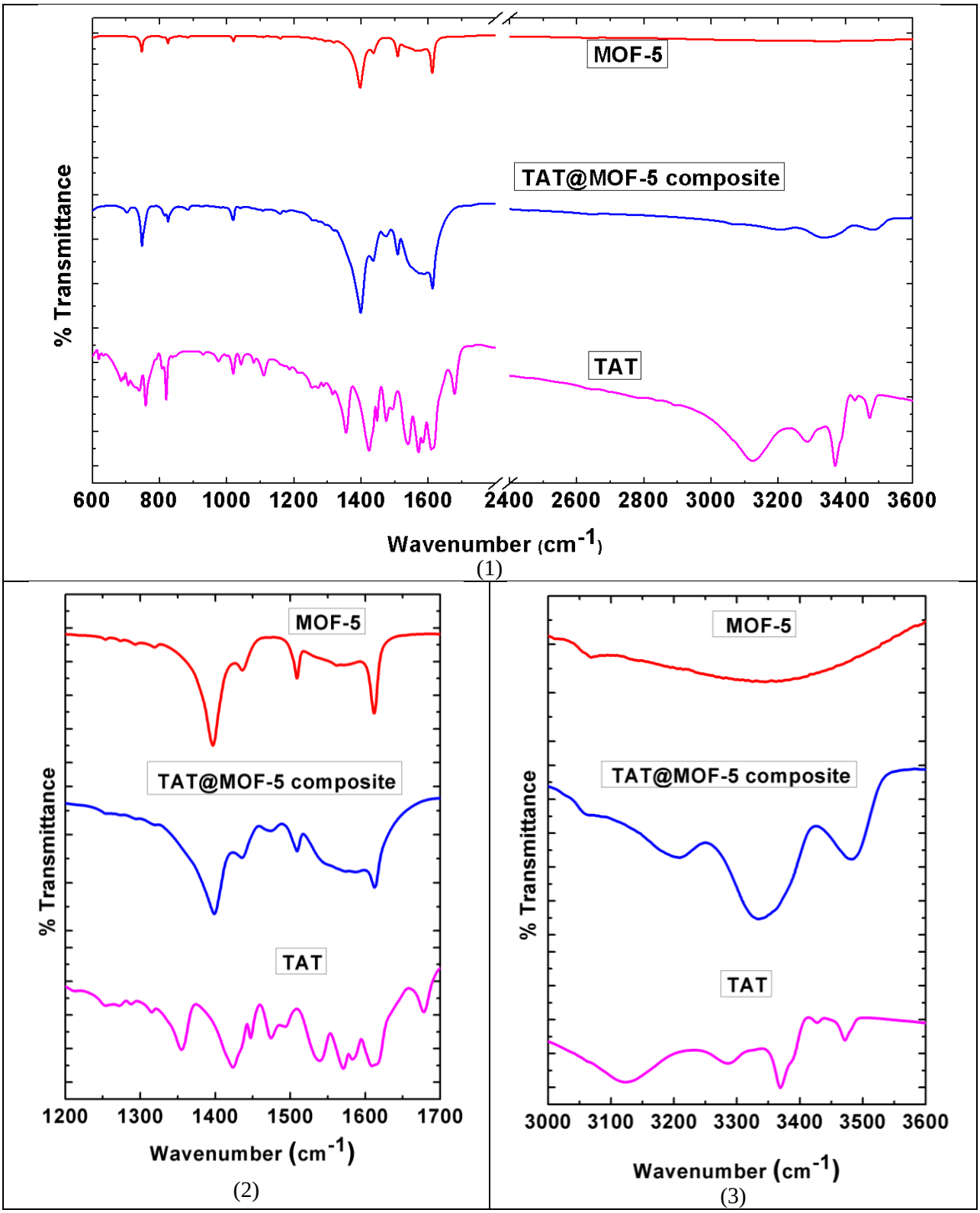

Figure S2c: (1) IR spectra of TAT@MOF-5 composite compared to MOF-5 and TAT. Figures (2) and (3) show specific spectral regions of the IR. Peaks corresponding to TAT and MOF-5 in a TAT@MOF-5 composite show strong similarities when compared to the starting components, although peak shifts are evident in MOF-5 as well as for TAT.

SI 5. Raman spectra of drug@MOF-5 composites compared with their starting components (Figure S3a-b)

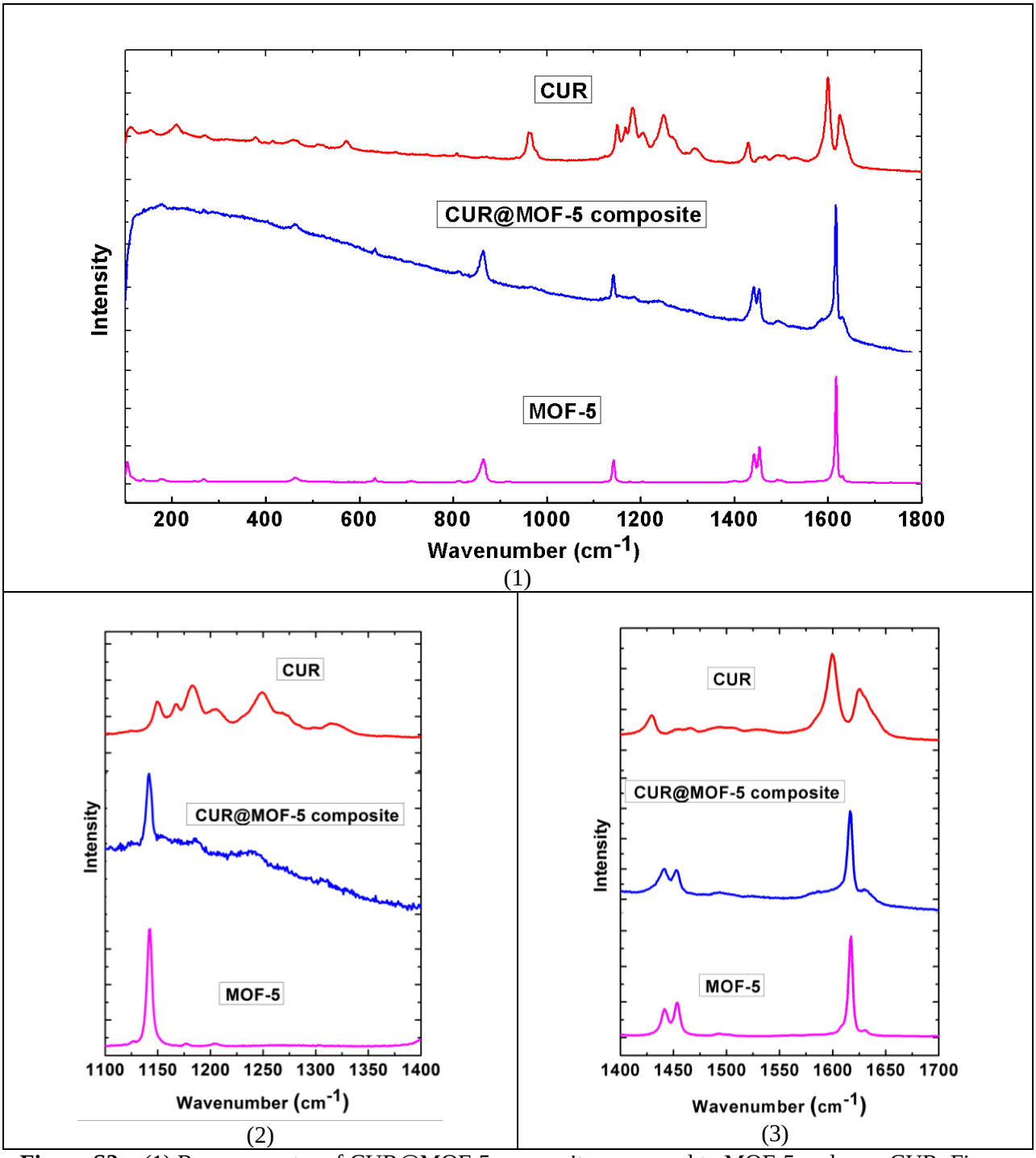

Figure S3a: (1) Raman spectra of CUR@MOF-5 composite compared to MOF-5 and pure CUR. Figures (2) and (3) show specific spectral regions of the Raman. Peaks corresponding to CUR and MOF-5 in a CUR@MOF-5 composite show strong similarities when compared to the starting components, although peak shifts are evident in MOF-5 as well as for CUR.

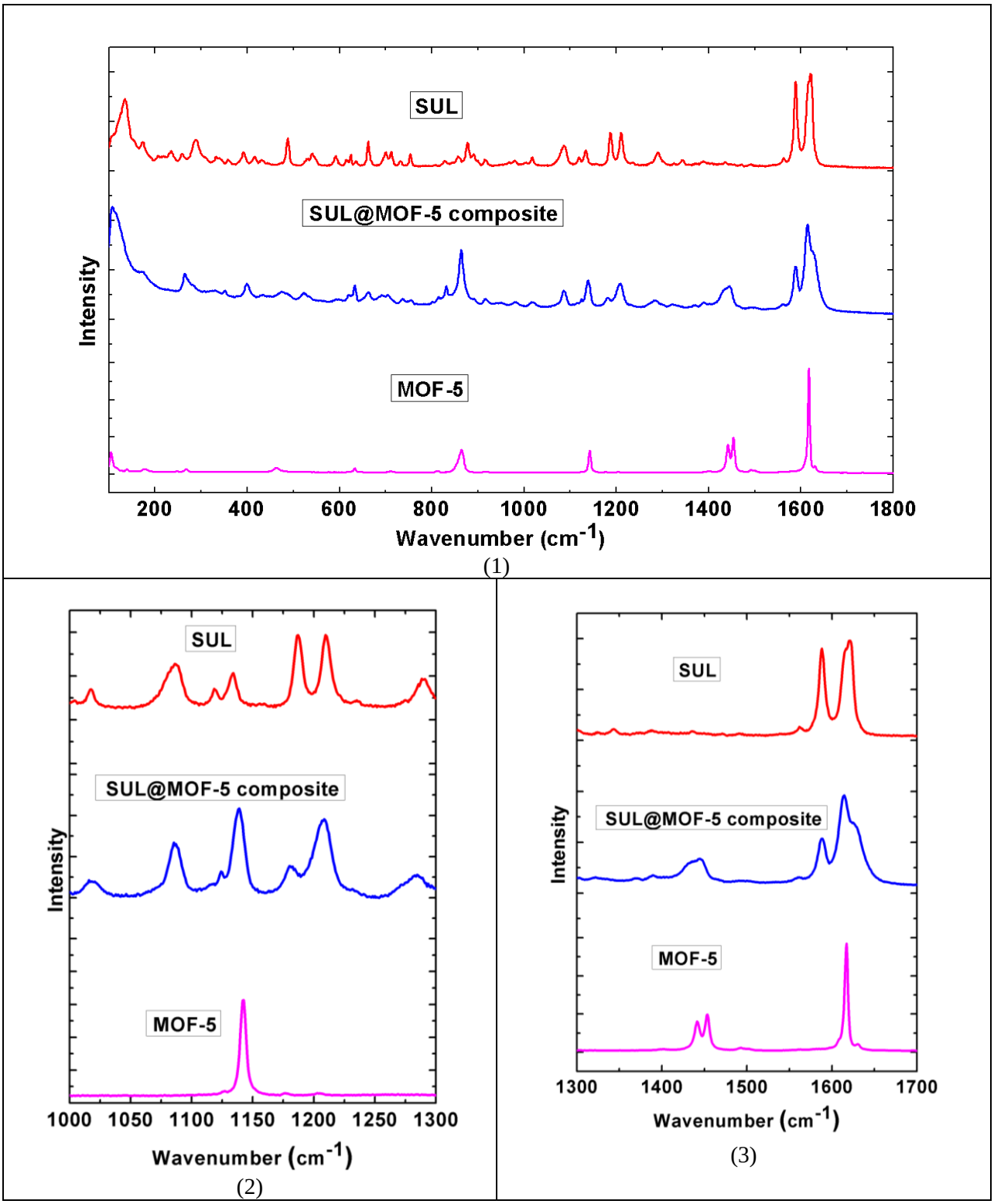

Figure S3b: (1) Raman spectra of SUL@MOF-5 composite compared to MOF-5 and pure SUL. Figures (2) and (3) show specific spectral regions of the Raman. Peaks corresponding to SUL and MOF-5 in a SUL@MOF-5 composite show strong similarities when compared to the starting components, although peak shifts are evident in MOF-5 as well as for SUL.

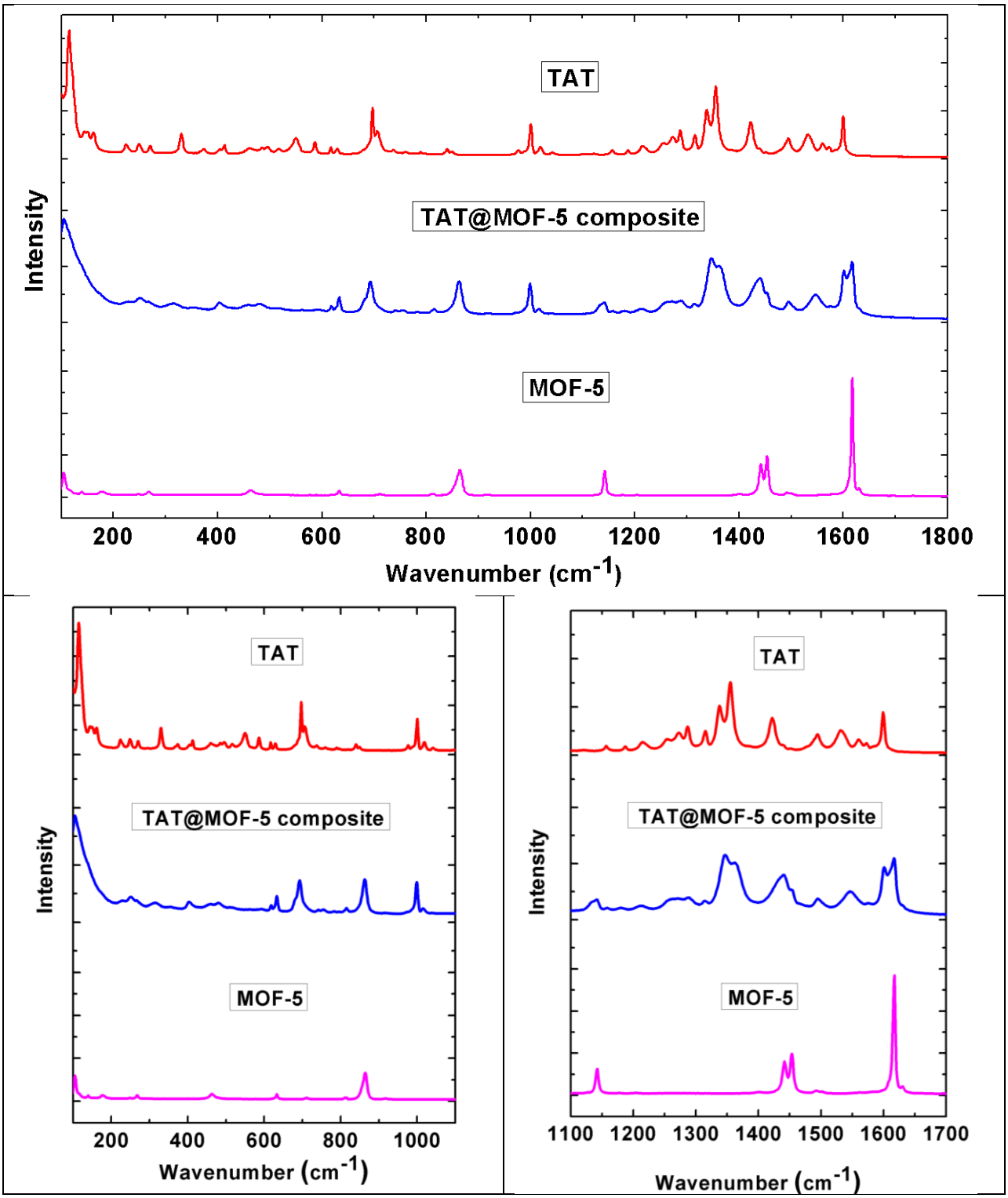

Figure S3c: (1) Raman spectra of TAT@MOF-5 composite compared to MOF-5 and pure TAT. Figures (2) and (3) show specific spectral regions of the Raman. Peaks corresponding to TAT and MOF-5 in a TAT@MOF-5 composite show strong similarities when compared to the starting components, although peak shifts are evident in MOF-5 as well as for TAT.

SI 6. IR and Raman frequency vibrational modes for the studied drug@MOF-5 composites and their starting components (Table S1)

Table S1: Selected Infrared and Raman frequency vibrational modes for the MOF-5, drug@MOF-5 composites, and drug molecules (CUR, SUL, and TAT)

MOF-5 (cm^{-1})	CUR@MOF-5 composite (cm^{-1})	CUR (cm^{-1})	SUL@MOF-5 composite (cm^{-1})	SUL (cm^{-1})	TAT@MOF-5 composite (cm^{-1})	TAT (cm^{-1})
ATR-IR spectroscopy analysis						
3069, 2649, 1611, 1562, 1508, 1436, 1396, 1319, 1293, 1253, 1159, 1020, 824, 746, 576, 518.	**MOF-5:** 3070, 2651, 1611, 1582, 1508, 1430, 1396, 1158, 1020, 824, 746, 576, 518. **CUR:** 3509, 3070, 3015, 2976, 2945, 1283, 1234, 1207, 1182, 977, 964, 885, 855, 814, 598. (a few peaks of CUR overlap with MOF-5 peaks)	3510, 3070, 3016, 2976, 2946, 1626, 1601, 1507, 1456, 1428, 1314, 1275, 1275, 1232, 1205, 1152, 977, 963, 855, 814, 600.	**MOF-5:** 3064, 2652, 1611, 1575, 1508, 1434, 1397, 1294, 1254, 1159, 1019, 824, 747, 577, 519. **SUL:** 3103, 3000, 2920, 1677, 1467, 1202, 1137, 1084, 917, 828. (a few peaks of SUL overlap with MOF-5 peaks)	3085, 3061, 3004, 2914, 1697, 1490, 1470, 1209, 1134, 1087, 917, 828.	**MOF-5:** 1612, 1509, 1435, 1398, 1019, 824, 747, 520. **TAT:** 3481, 3334, 3208, 1587, 1474, 1040, 1019, 815. (a few peaks of TAT overlap with MOF-5 peaks)	3471, 3369, 3285, 3122, 1675, 1608, 1583, 1570, 1539, 1423, 1042, 1019, 819, 758, 545.
Raman spectroscopy analysis						
1617, 1453, 1441 1142, 864, 633, 464.	**MOF-5:** 1616, 1452, 1440, 1142, 863, 464. **CUR:** 1626, 1595, 1238, 1186, 1170, 464. (a few peaks of CUR overlap with MOF-5 peaks)	1627, 1599, 1429, 1318, 1249, 1183, 1167, 1150, 964, 572, 379, 209, 155.	**MOF-5:** 1615, 1440, 1138, 864, 633, 462. **SUL:** 1615, 1588, 1208, 1115, 1086, 392, 170, 107. (a few peaks of SUL overlap with MOF-5 peaks)	1621, 1588, 1209, 1118, 1086, 877, 662, 488, 399, 290, 175, 134.	**MOF-5:** 1616, 1438, 1138, 863, 633, 458. **TAT:** 1600, 1546, 1354, 999, 863, 692, 315, 107. (a few peaks of SUL overlap with MOF-5 peaks)	1599, 1532, 1422, 1355, 1000, 697, 550, 330, 115.

SI 7. N_2 gas adsorption-desorption isotherms of MOF-5 and drug@MOF-5 composites

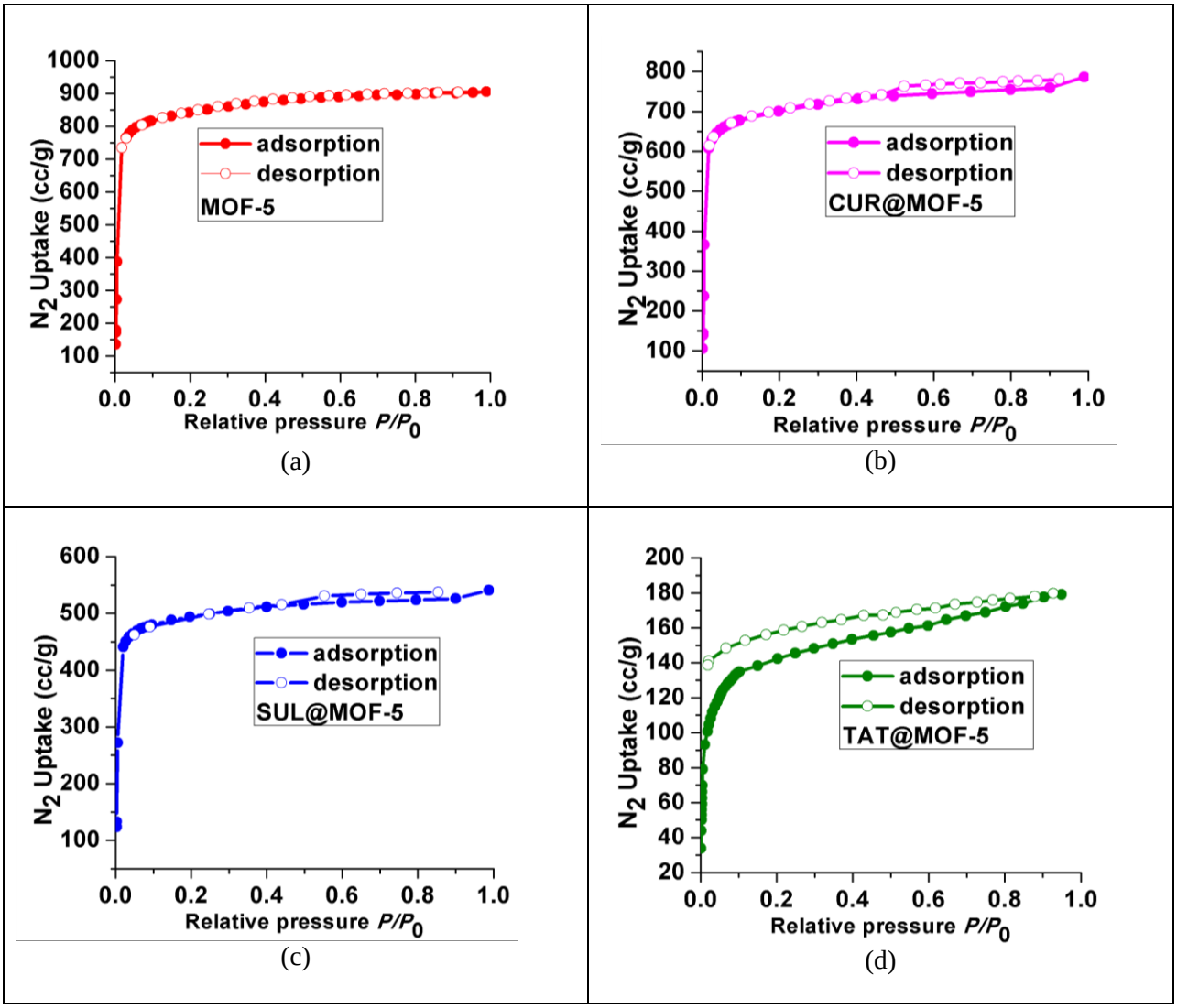

Figure S4a-d: N_2 gas adsorption-desorption isotherms of MOF-5 (a) CUR@MOF-5 (b), SUL@MOF-5 (c), and TAT@MOF-5 (d) composites show maintenance of substantial surface area after encapsulation of drug molecules.

SI 8. Drug encapsulation (wt%) was quantified by UV-vis spectroscopy

Weight percentage (wt%) of the incorporated drug in drug@MOF-5 composite was determined using UV-vis spectroscopy ((HP, Agilent 8453 UV-Visible Spectrophotometer) on digested samples (in methanol:1N hydrochloric acid (3:1, v/v) media) by quantifying absorbance at λ_{max} 420 nm for CUR, λ_{max} 330 nm for SUL, and λ_{max} 368 nm for TAT respectively. First, standard solutions of known concentrations of CUR or SUL or TAT were prepared in a methanol:1N hydrochloric acid (3:1, v/v) media and these standard solution absorbance values were recorded and used to create calibration curve. These curves were used to determine the unknown concentration of CUR or SUL or TAT in the drug@MOF-5 composites: 7.7 wt% of CUR, 22.4 wt % of SUL, and 34.0 wt% encapsulated in MOF-5 respectively (wt% calculated based on the drug composite).

Table S2. Drug content per cage in a MOF-5

Compound name	Drug per cage	Drug weight percentage
CUR@MOF-5	0.18	7.7%
SUL@MOF-5	0.66	22.4%
TAT@MOF-5	1.51	34.0%

SI 9. Simulated gastric (SG) and phosphate buffer media (PBS) preparation

SG media (pH 1.2) preparation: Sodium chloride (NaCl, 2.00 g) and hydrochloric acid (36.5-38.0%, w/w, 8.2 mL) were dissolved in 1L deionized water at room temperature.
PBS (pH 7.4) preparation: Sodium chloride (NaCl, 8.00 g), dibasic sodium phosphate (Na_2HPO_4, 1.44 g), monobasic potassium phosphate (KH_2PO_4, 0.24 g), and potassium chloride (KCl, 0.20 g) were dissolved in 1L ionized water at room temperature and the pH adjusted with 1N hydrochloric acid.
Methylcellulose (0.5 wt%) polymer added SG media preparation: Methylcellulose (0.05g) was dissolved in 100 mL SG media in a 250 mL beaker and heated at 40 °C for 5 min with agitation. Then beaker was placed in a beaker (1L) contains ice water for 20 min to get homogenous media.
Methylcellulose (0.5 wt%) polymer added PBS media preparation: Methylcellulose (0.05g) was dissolved in 100 mL PBS media in a 250 mL beaker and heated at 40 °C for 5 min with agitation. Then beaker was placed in a beaker (1L) contains ice water for 20 min to get homogenous media.

SI 10. MOF-5 and drug@MOF-5 composite decomposition study in dissolution media
MOF-5 decomposition was confirmed by soaking ~20 mg MOF-5 crystals and drug@MOF-5 composites (CUR@MOF-5, SUL@MOF-5, and TAT@MOF-5) in SG and PBS media respectively. These solutions were stirred at 200 rpm using magnetic stir bars at 37 °C. Visibly MOF-5 and drug@MOF-5 composites crystals burst into powder within a few minutes in both media, demonstrating that the MOF-5 framework collapsed/digests and chemically transformed into by-products. After 4 hours, the suspensions were filtered and dried at room temperature then the solids are analyzed by PXRD. It was observed that the MOF-5 and drug@MOF-5 composites in SG media yielded terephthalic acid whereas PBS media resulted in Zn-terephthalate-dihydrate salt[3] precipitate including other decomposition products.[4]

SI 11. PXRD patterns of MOF-5 decomposition products in dissolution media (Figure S5a-b)

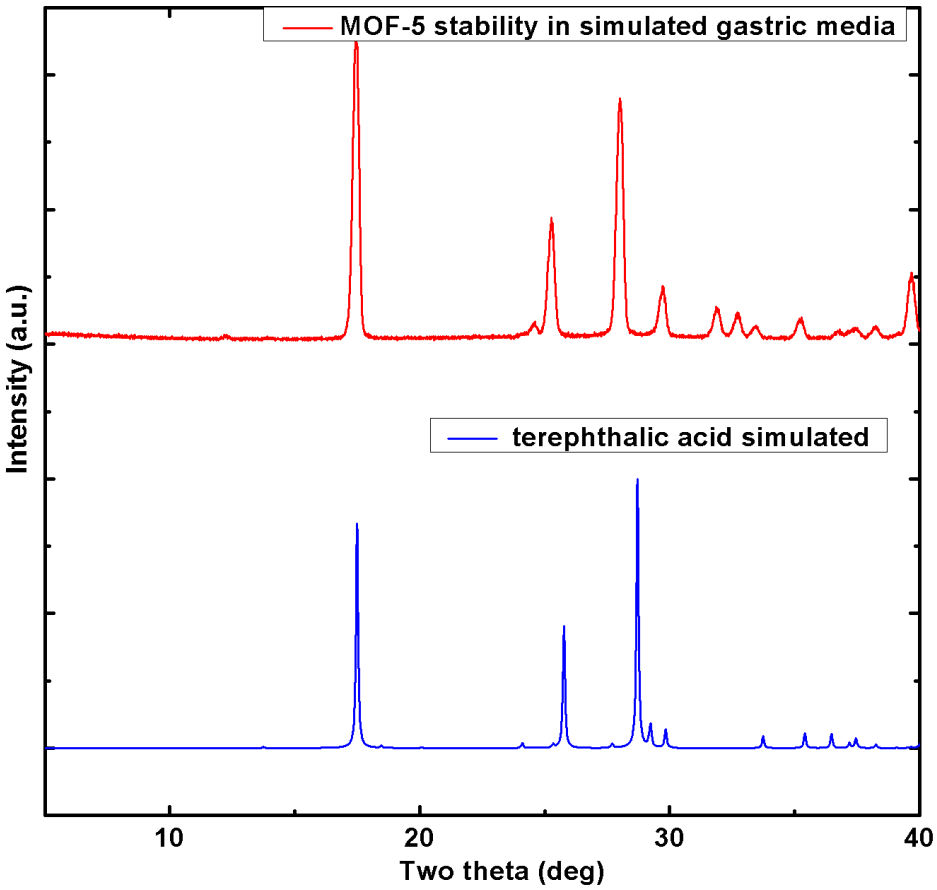

Figure S5a: MOF-5 decomposed product PXRD pattern compared with terephthalic acid simulated pattern extracted from crystal structure (Refcode- TEPHTH16).[5]

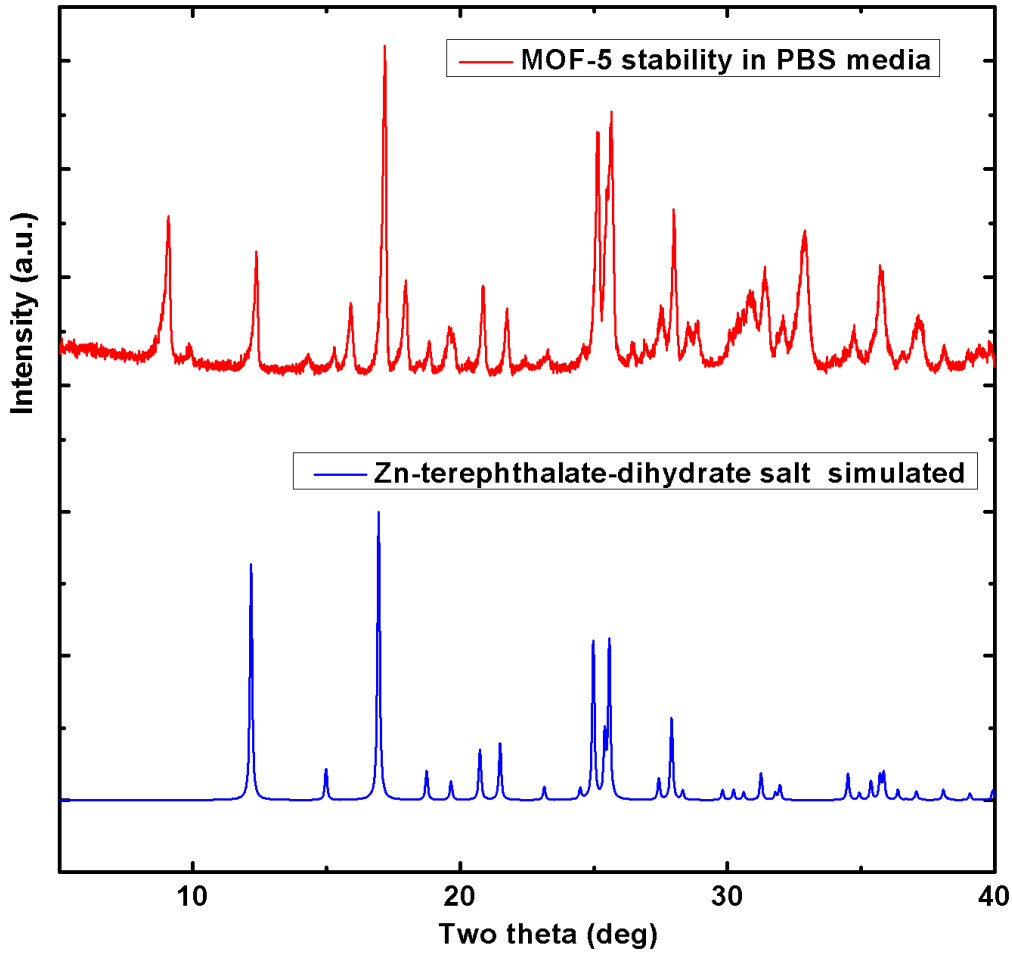

Figure S5b: MOF-5 decomposed product PXRD pattern compared with Zn-terephthalate-dihydrate salt simulated pattern extracted from crystal structure (Refcode- DIKQET).[4] Additonal phases are also present.

SI 12. PXRD patterns of drug@MOF-5 composites decomposition products in dissolution media (Figure S6a-d)

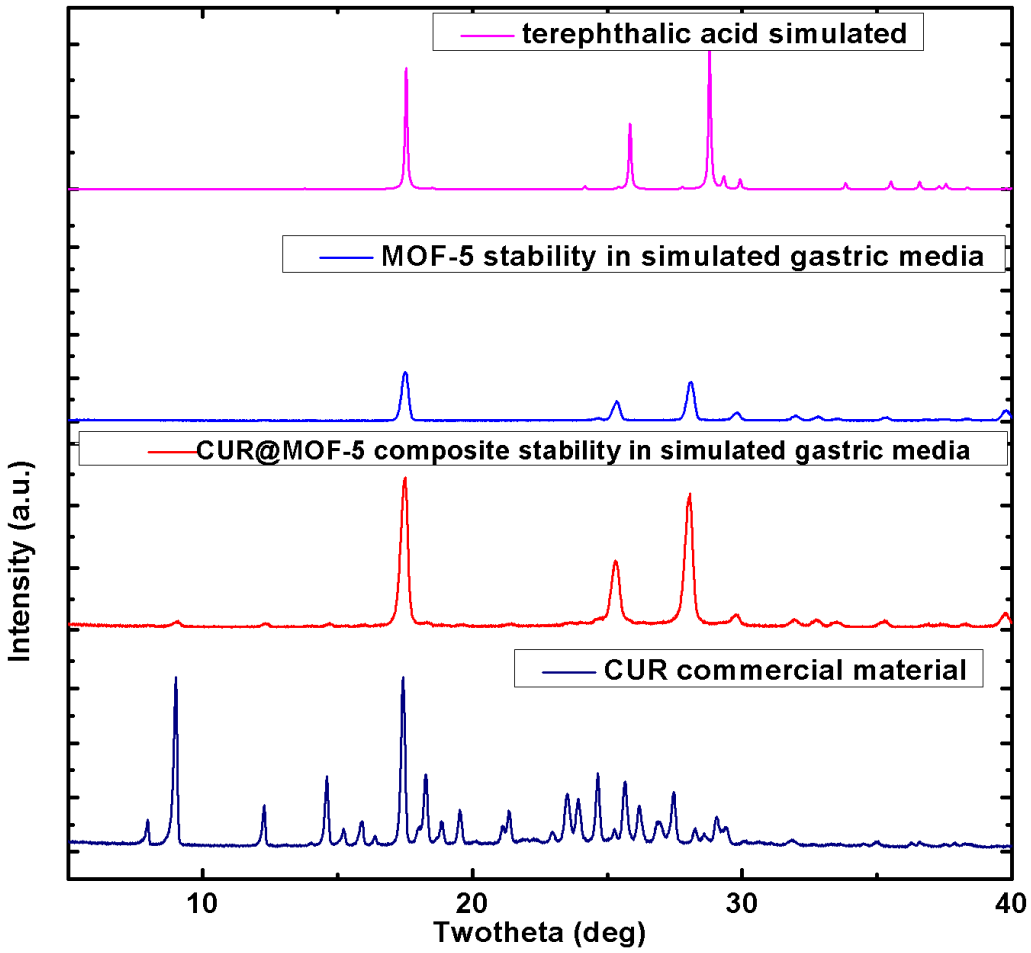

Figure S6a: CUR@MOF-5 composite decomposed product PXRD pattern compared with terephthalic acid simulated pattern extracted from crystal structure indicating that decomposition behavior is akin to pure MOF-5. Additionally, diffraction lines belong to pure CUR are also observed and compared with pure CUR powder pattern.

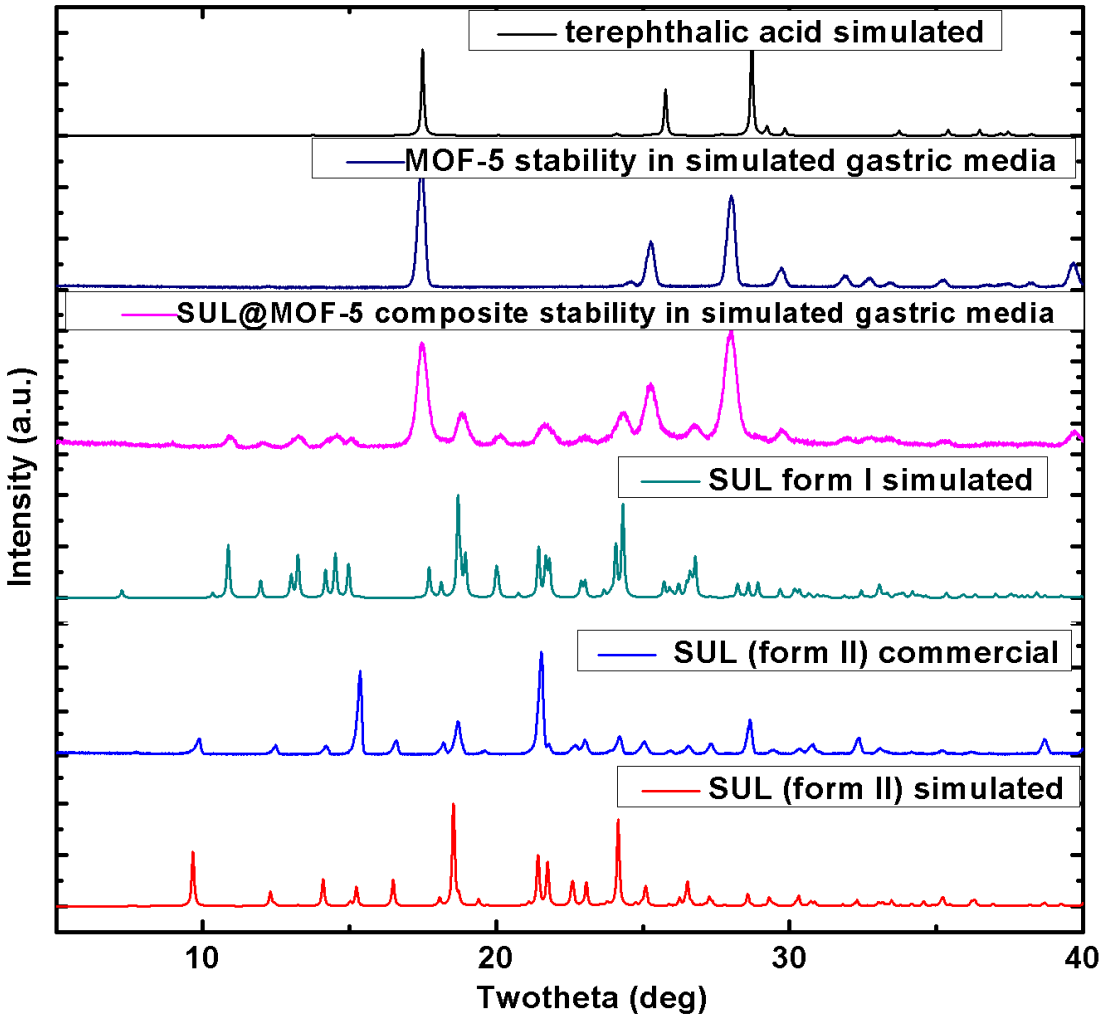

Figure S6b: SUL@MOF-5 composite decomposed product, PXRD pattern compared with terephthalic acid simulated pattern extracted from crystal structure indicating that decomposition behavior is akin to pure MOF-5. Similarly, diffractions lines belong to SUL form I (monoclinic) are also observed which is compared with SUL form I (monoclinic) and form II (orthrhomibic) simulated patterns extracted from crystal structures.[6]

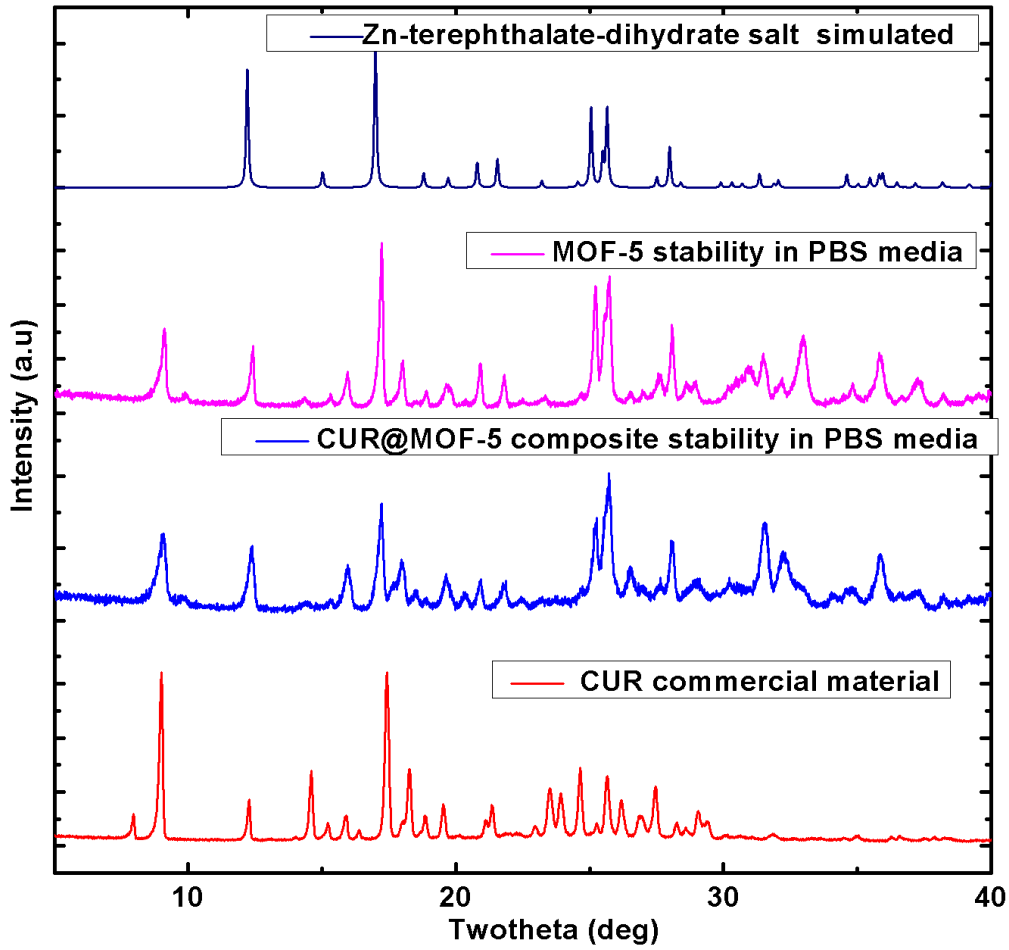

Figure S6c: CUR@MOF-5 composite decomposition in PBS media resulted in Zn-terephthalate-dihydrate salt dihydrate including other decomosition products which was confirmed by PXRD and it was compared with pure MOF-5 digestion in PBS media and Zn-terephthalate-dihydrate simulated pattern extracted from crystal structure[4] as well as pure CUR powder pattern.

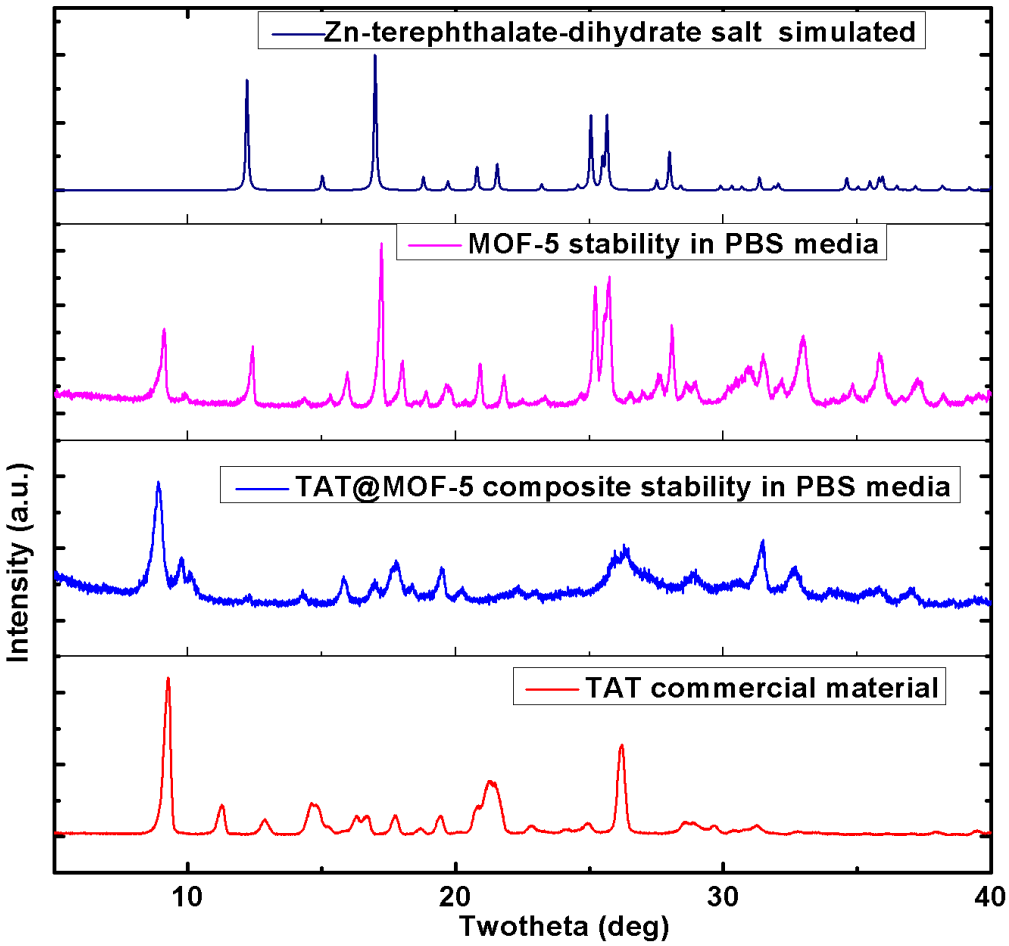

Figure S6d: TAT@MOF-5 composite decomposition in PBS media resulted in Zn-terephthalate-dihydrate including other decomposition products which was confirmed by PXRD and it was compared with pure MOF-5 digestion in PBS media and Zn-terephthalate-dihydrate simulated pattern extracted from crystal structure as well as pure TAT powder pattern.

SI 13. PXRD patterns of CUR and SUL stability in dissolution media (Figure S7a-d)

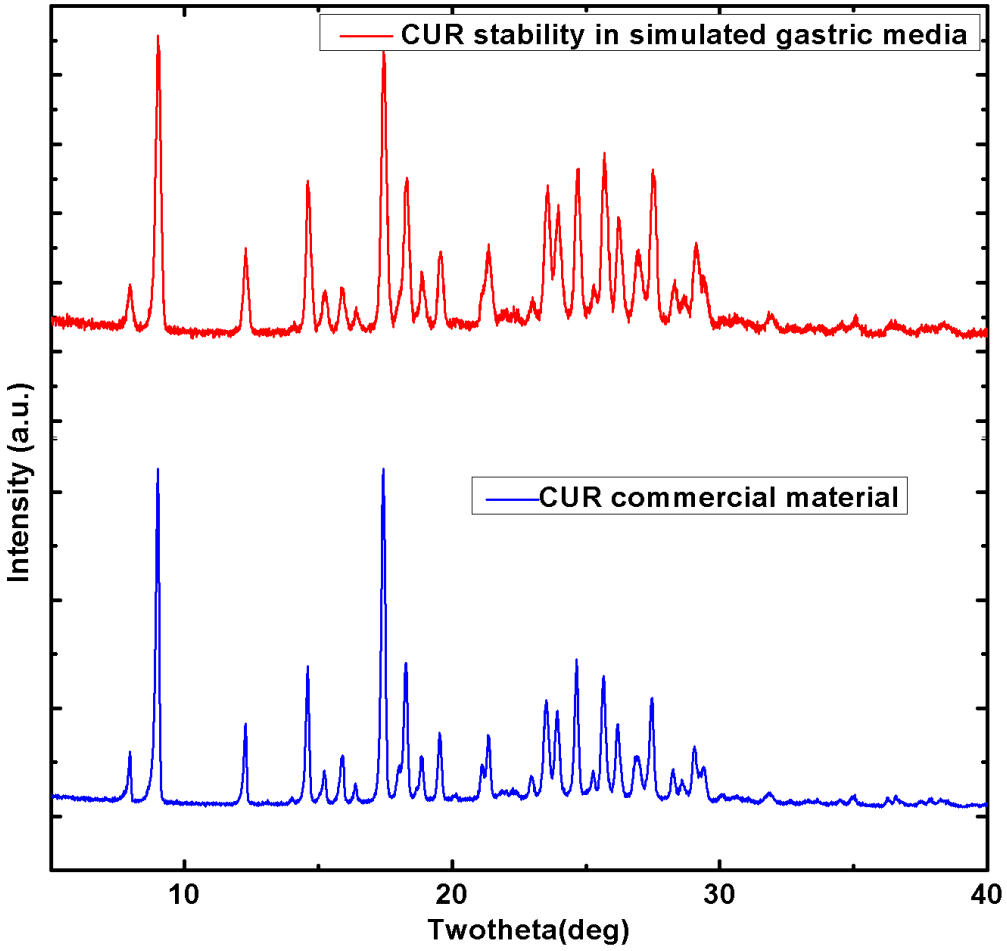

Figure S7a: The undissolved material obtained from CUR excess solid added into gastric media, which is compared with starting CUR shows good match indicates that CUR stable under simulated gastric conditions.

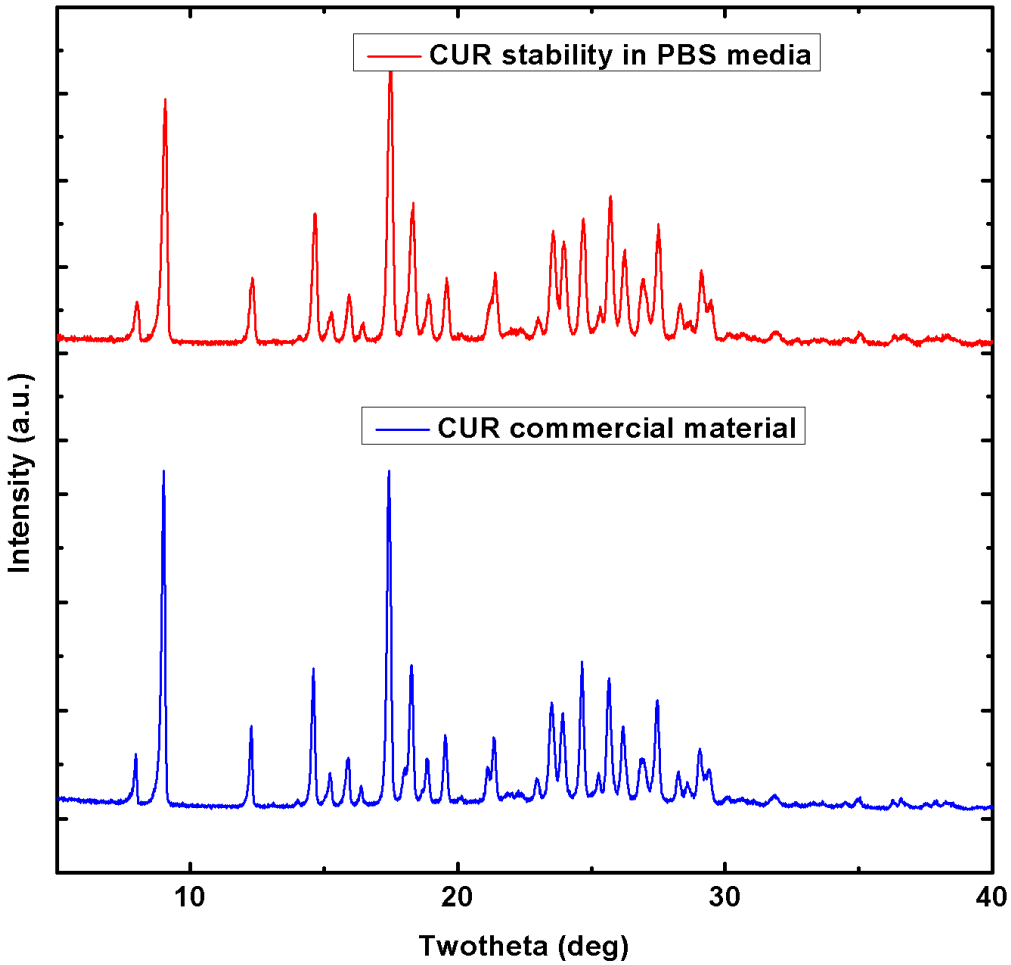

Figure S7b: The undissolved material obtained from CUR excess solid added into PBS media, which is compared with starting CUR shows good match indicates that CUR stable in PBS media.

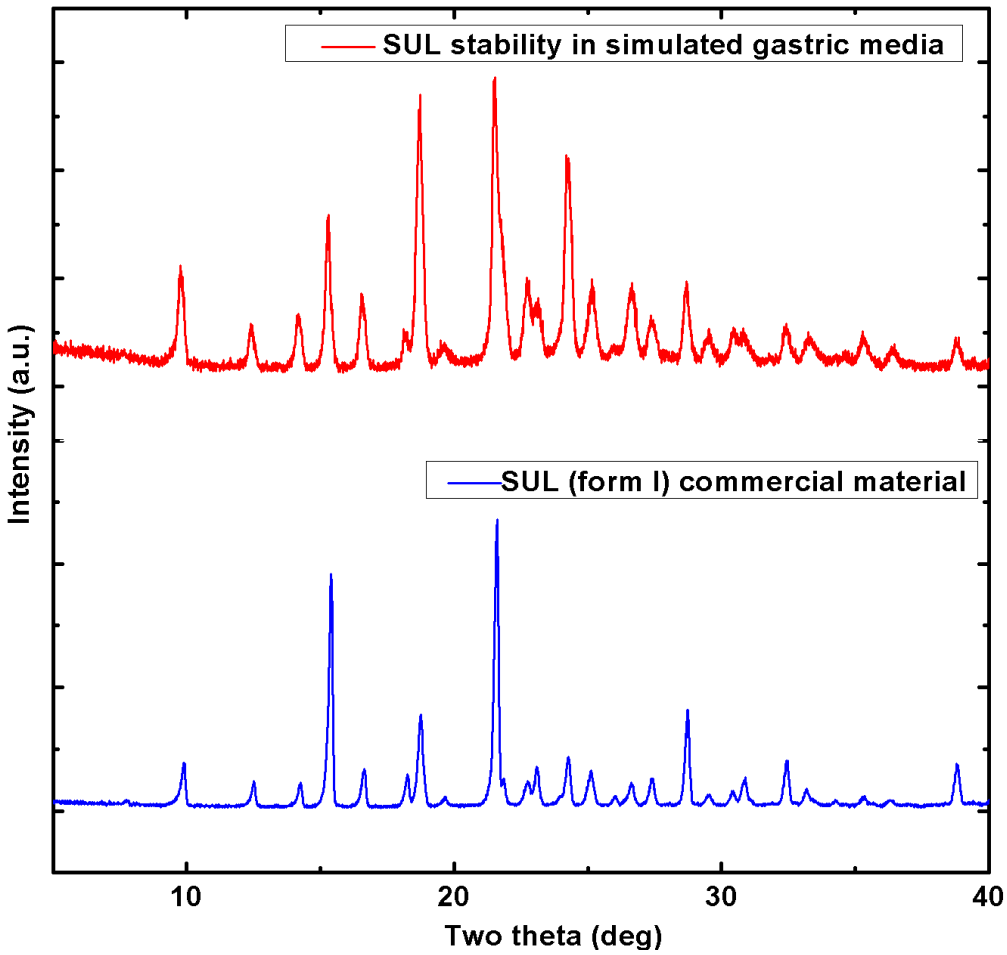

Figure S7c: The undissolved material obtained from SUL excess solid added into gastric media, which is compared with starting SUL shows good match indicates that SUL stable under simulated gastric media.

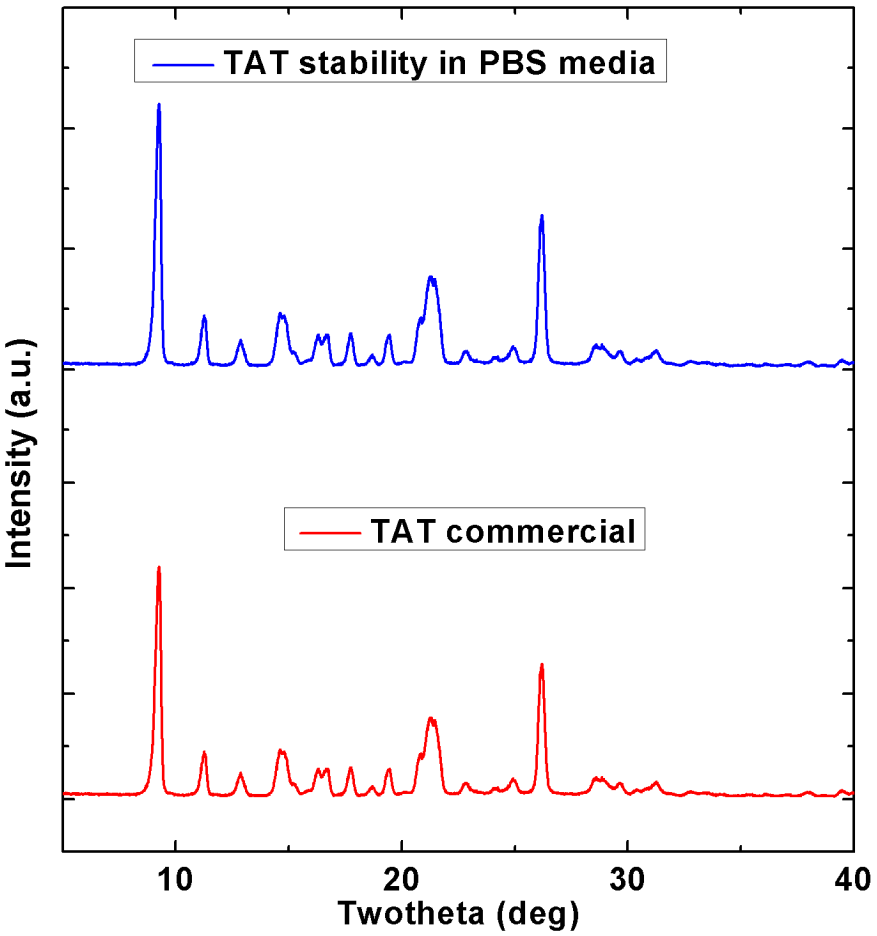

Figure S7d: The undissolved material obtained from TAT excess solid added into PBS media, which is compared with starting TAT shows good match indicates that TAT stable under simulated PBS media.

S14. Dissolution studies

Dissolution of drug@MOF-5 composites, physical mixtures of components, pure SUL, CUR, and TAT were measured with a Pion Rainbow Dynamic Dissolution Monitor® system at 37 °C. Standard solutions of known concentrations were used to create calibration curves for each medium (simulated gastric and PBS media). All values collected during dissolution were compared to these calibration curves.

For CUR, and CUR@MOF-5 composite dissolution studies, ~1 mg of CUR and ~5 mg of CUR@MOF-5 composite and a physical mixture of components were added in 15 mL of solution medium individually, stirred at 200 rpm and UV-Vis probes with a path length of 10 mm were submerged above the stir bars. A time dependent concentration curve was observed in situ using the AuPRO software (Version 5.1.1.0). The lambda maximum for the absorbance of CUR is located at λ_{max} 420 nm for all three different solid forms in both media.

For SUL and SUL@MOF-5 composite dissolution studies, ~1mg of SUL and ~5mg of SUL@MOF-5 composite and a physical mixture of components were added in 15 mL of solution medium individually, stirred at 200 rpm and UV-Vis probes with a path length of 10 mm were submerged above the stir bars. A time dependent concentration curve was observed in situ using the AuPRO software (Version 5.1.1.0). The lambda maximum for the absorbance of SUL is located at λ_{max} 330 nm in both media.

For TAT and TAT@MOF-5 composite dissolution studies, ~1mg of TAT and ~5mg of TAT@MOF-5 composite and a physical mixture of components were added in 15 mL of solution medium individually, stirred at 200 rpm and UV-Vis probes with a path length of 10 mm were submerged above the stir bars. A time dependent concentration curve was observed in situ using the AuPRO software (Version 5.1.1.0). The lambda maximum for the absorbance of TAT is located at λ_{max} 368 nm in both media.

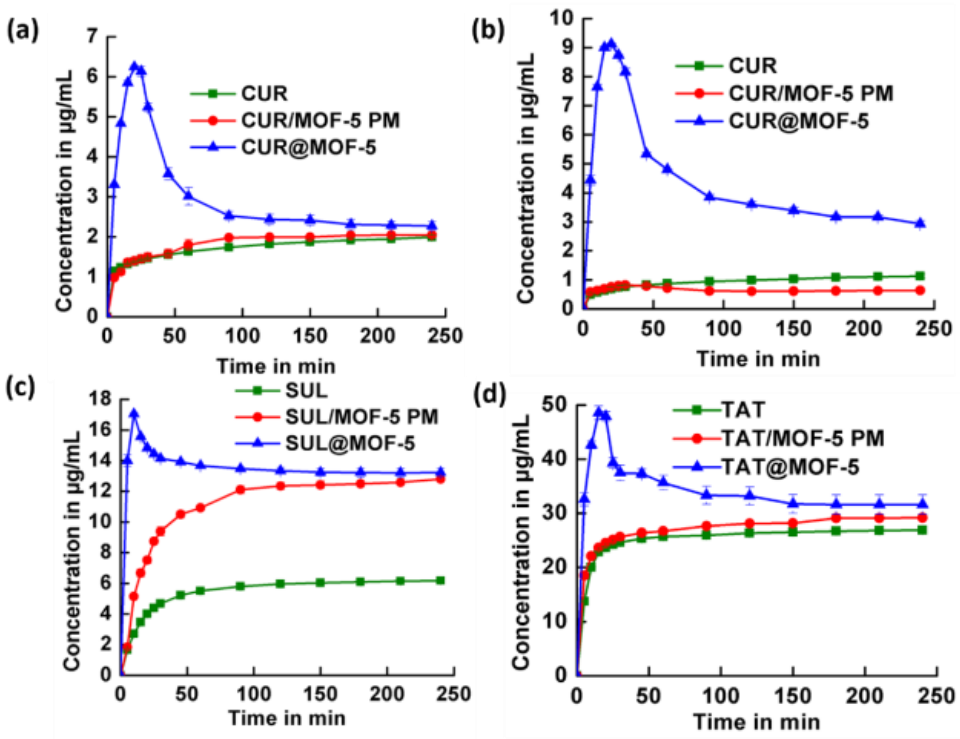

Figure S8: Representative CUR, CUR@MOF-5 composite and physical mixture dissolution profiles in simulated (a) gastric media and (b) PBS media. (c) Representative SUL, SUL@MOF-5 composite and physical mixture dissolution profiles in simulated gastric media and (c) Representative TAT, TAT@MOF-5 composite and physical mixture dissolution profiles in PBS media. Immediate release is observed, but concentration decreases after achieving a maximum due to drug precipitation, as is typical for a supersaturating drug delivery system without additives. Nonetheless the AUC is enhanced significantly and can further be improved with additives as shown in Figure 4.

Table S3: C_{max} and $AUC_{0\text{-}4}$ values (Average (Standard Error of the Mean)) of CUR, SUL, CUR@MOF-5, SUL@MOF-5, TAT@MOF-5 composites and their physical mixtures (PM) in SG and/or PBS media.

compound	C_{max} (µg/mL)		$AUC_{0\text{-}4}$ (mg*h/mL)	
	SG media	PBS media	SG media	PBS media
CUR	1.99(4)	1.12(7)	0.41(6)	0.22(3)
CUR/MOF-5 PM	2.04(4)	0.81(5)	0.44(5)	0.15(3)
CUR@MOF-5	6.24(3)	9.13(3)	0.70(6)	0.93(9)
	SG media		SG media	
SUL	6.01(6)		1.32(2)	
SUL/MOF-5 PM	12.80(14)		2.70(4)	
SUL@MOF-5	17.10(5)		3.20(41)	
	PBS media		PBS media	
TAT	26.79(15)		6.09(8)	
TAT/MOF-5 PM	30.23(65)		6.74(10)	
TAT@MOF-5	48.53(74)		8.11(10)	

SI 15. Stability

CUR@MOF-5 and SUL@MOF-5 composites were stored in a N_2 filled glove box and analyzed after 4 months by PXRD. No degradation of MOF-5 was observed and diffraction peaks corresponding to the crystalline drug molecules were absent indicating that the both CUR@MOF-5 and SUL@MOF-5 drug composites are stable up to at least 4 months.

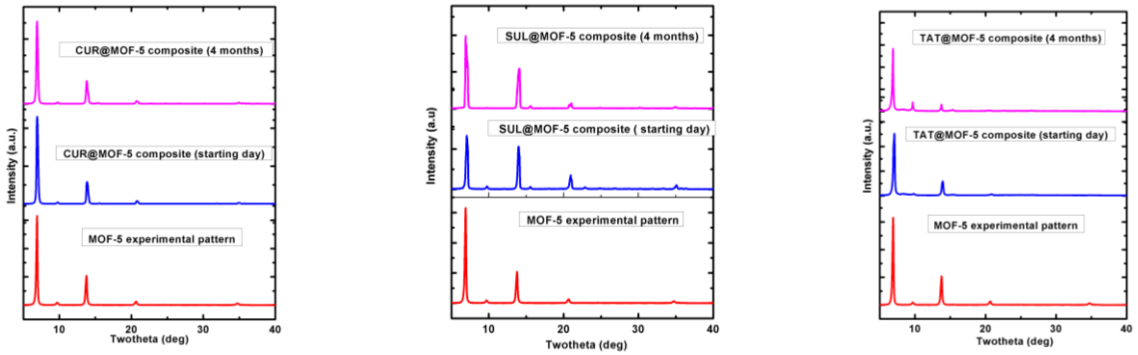

(a) (b) (c)

Figure S9: Stability of drug@MOF-5 composites over time. (a) CUR@MOF-5, (b) SUL@MOF-5 (c) TAT@MOF-5 composites compared to MOF-5 experimental pattern.

SI 16. References:

1. H. Li, M. Eddaoudi, M. O'Keeffe, O. M. Yaghi, Design and synthesis of an exceptionally stable and highly porous metal-organic framework. *Nature* **1999**, *402*, 276-279.
2. Jade Plus 8.2 ed.; Materials Data, Inc. 1995-2007.
3. K. A. Cychosz, A. J. Matzger, Water stability of microporous coordination polymers and the adsorption of pharmaceuticals from water. *Langmuir*, **2010**, *26(22)*, 17198-17202.
4. G. Guilera, J. W. Steed, Topological control in coordination polymers by non-covalent forces. *Chem. Commun*., **1999**, *0*, 1563-1564.
5. D. P. Karothu, J. Weston, I. T. Desta, P. Naumov, Shape-Memory and Self-Healing Effects in Mechanosalient Molecular Crystals. *J. Am. Chem. Soc*., **2016**, *138*, 13298-13306.
6. A. L.Grzesiak, A. J. Matzger, New form discovery for the analgesics flurbiprofen and sulindac facilitated by polymer-induced heteronucleation. *J. Pharm. Sci.*, **2007**, *96*, 2978-2986.